Journal of Mathematical Imaging and Vision 15: 39–53, 2001

Non-Linear Scale-Spaces Isomorphic to the Linear Case with Applications to Scalar, Vector and Multispectral Images

LUC FLORACK
Department of Mathematics, Utrecht University, Budapestlaan 6, NL-3584 CD Utrecht, The Netherlands
Luc.Florack@math.uu.nl

Abstract. A basic requirement of scale-space representations in general is that of scale causality, which states that local extrema in the image should not be enhanced when resolution is diminished. We consider a special class of nonlinear scale-spaces consistent with this constraint, which can be linearised by a suitable isomorphism in the grey-scale domain so as to reproduce the familiar Gaussian scale-space. We consider instances in which nonlinear representations may be the preferred choice, as well as instances in which they enter by necessity. We also establish their relation to morphological scale-space representations based on a quadratic structuring function.

Keywords: linear/nonlinear/morphological scale-space theory, scalar/vector/multispectral imagery

1. Introduction

A *scale-space representation* [7, 9, 11, 14, 17, 22, 24, 25] is an embedding of an image into a parametrised family, in which the parameter encodes scale or resolution (coarse/fine scale means low/high resolution, respectively). Koenderink has argued that in order for such an embedding to be a sensible one it must satisfy a basic causality condition: Local extrema should not be enhanced as resolution is diminished. In other words, if image intensity is locally maximal (minimal), its derivative with respect to scale should be nonpositive (nonnegative, respectively). (This poses no constraint on the number of extrema. In particular, extrema may be created as resolution is diminished, as long as they satisfy the non-enhancement property). He subsequently narrows down the solution space by imposing plausible symmetry constraints, notably isotropy, homogeneity, and linearity. This uniquely establishes a linear representation known as *Gaussian scale-space*.

In this article we consider generalised representations by relaxing the additional demands, notably linearity, and discuss a number of potential applications in which the standard Gaussian case may not be appropriate or may even be inconsistent. The theory is applicable to scalar, vector and multispectral images. We also establish a relationship between the resulting nonlinear representation for scalar images and particular types of scale-space constructs encountered in mathematical morphology, viz. those obtained by erosion and dilation by quadratic structuring functions of variable width.

2. Theory

Let $f(x)$ be an image defined on some compact subset of $\mathbb{R}^n$, and consider its embedding into a family of functions of the type $u(x; s)$ with $(x; s) \in \mathbb{R}^n \times \mathbb{R}^+$, such that $\lim_{s\downarrow 0} u(x; s) = f(x)$, say. Let us assume for the moment that the fiducial origin corresponds to a local extremum of u at some arbitrary level of scale. In order to enforce the scale causality condition, the scale derivative (at the origin) must be such that the value of u is not enhanced.

If u is continuously differentiable with respect to s and twice continuously differentiable with respect to

x, then the osculating paraboloid to an iso-surface in scale-space at a spatial extremum—the origin, say—is given by

$$s = \frac{1}{2} x^{\mathrm{T}} \mathbf{Q} x \quad \text{with} \quad \mathbf{Q} = -\frac{1}{u_s} \mathbf{H}. \tag{1}$$

Here, $\mathbf{H}$ is the Hessian matrix of u evaluated at the origin, with entries u_{ij}, $i, j = 1, \ldots, n$ (second order *spatial* derivatives of u), and u_s is the scale derivative of u. Note that in an extremum the Hessian eigenvalues are either all positive or all negative, so that the corresponding surface is indeed a paraboloid. At the origin its normal coincides with the normal to the original iso-surface, and points towards increasing scale if and only if

$$u_s \Delta u > 0. \tag{2}$$

To see this, note that the sign of all Hessian eigenvalues equals that of their sum, i.e. the Laplacean. Vice versa, if $u_s \Delta u > 0$ at extrema irrespective of the image, then u_s has locally the same signature as (each eigenvalue of) the Hessian matrix, so that Eq. (1) defines a paraboloid pointing upward.

The simplest *linear* p.d.e. that realises the constraint Eq. (2) is the isotropic diffusion equation. Endowed with initial condition the scale-space defining p.d.e. system then becomes

$$\begin{cases} \partial_s u = \Delta u, \\ \lim\limits_{s \to 0} u = f, \end{cases} \tag{3}$$

but note that the addition of terms of the form $\mathcal{O}(\nabla u)$ on the r.h.s. of the p.d.e. does not violate the causality principle. Equation (3) has a closed-form solution, viz. u can be obtained from f by convolving it with a normalised Gaussian of width $\sigma = \sqrt{2s}$. This is an important observation that will be exploited in all subsequent considerations.

Suppose that we have reasons to consider an alternative parametrisation,

$$u \stackrel{\text{def}}{=} \gamma(v) \quad \text{with} \quad \gamma' > 0 \tag{4}$$

say. (From a mathematical point of view there is no compelling reason to prefer any particular parametrisation in view of isomorphism, but there may be physical arguments to do so, *v.i.*) Let the functional $\gamma\mathbf{Q}$ denote the coefficient matrix of Eq. (1) evaluated for the reparametrised image, i.e. $\gamma\mathbf{Q}[\gamma^{\text{inv}}(u)] = \mathbf{Q}[u]$. Then clearly $\gamma\,\mathbf{Q} = \mathbf{Q}$ at the location of a critical point ($\nabla u = 0$). In particular we may conclude that at extrema the convex side of a scale-space iso-surface still points in the direction of increasing scale. In other words, monotonic grey-scale mappings of the type $u = \gamma(v)$ preserve the causality property. Combining Eq. (4) with Eq. (3) yields the following nonlinear initial value problem for v:

$$\begin{cases} \partial_s v = \Delta v + \mu \|\nabla v\|^2, \\ \lim\limits_{s \to 0} v = g. \end{cases} \tag{5}$$

in which the nonlinearity is defined by

$$\mu \stackrel{\text{def}}{=} (\ln \gamma')', \tag{6}$$

and the initial condition by

$$g \stackrel{\text{def}}{=} \gamma^{-1}(f). \tag{7}$$

To see this, substitute Eqs. (4) into (3), and divide by γ', which is allowed by virtue of the monotonicity property. The right hand side of the p.d.e. in Eq. (5) generalises the familiar Laplacean by taking the parametrisation degree of freedom of its operand v into account via the nonlinearity μ. In arbitrary metric spaces and expressed in parametrisation independent ("covariant") form the Laplacean is also known as the *Laplace–Beltrami operator*, *cf.* Kimmel et al. (1999). The covariant form of the p.d.e. in Eq. (5) is given by the following corollary, valid in an arbitrary parametrisation.

Corollary 1 (*Covariant Formulation*)**.** *If we account for an arbitrary parametrisation and general choice of metric, Eq.* (5) *can be written as*

$$\partial_t v = \frac{1}{\sqrt{\eta}} \nabla_\alpha \left(\sqrt{\eta} \eta^{\alpha\beta} \nabla_\beta v \right) + \mu\, \eta^{\alpha\beta} \nabla_\alpha v \nabla_\beta v,$$

in which $\eta_{\alpha\beta}$ are the components of the metric tensor, with inverse $\eta^{\alpha\beta}$ and determinant η.

Proof: If we take $\eta_{\alpha\beta} = \delta_{\alpha\beta}$, i.e. 1 if $\alpha = \beta$ and 0 otherwise (the usual Euclidean metric), and if we set $t = \sqrt{\eta}\, s$, then the above equation takes the form of Eq. (5). Since the r.h.s. of the equation in the corollary is a tensor (cf. Misner et al., [19] for details), it

is valid in any coordinate system. In fact, it can be generalised to any metric space by taking an appropriate choice of metric $\eta_{\alpha\beta}$, not necessarily Euclidean (in that case its form cannot be reduced to that of Eq. (5) however). □

The first term on the right hand side in Corollary 1 is the spatial coordinate independent Laplace—Beltrami operator acting on the image function, the second term generalises it so as to make it greyvalue parametrisation independent in addition.

We have the following commuting diagram:

$$\begin{array}{ccc} u & \xleftarrow{\gamma} & v \\ Eq.\ (3) \uparrow & & \uparrow\ Eq.\ (5) \\ f & \xrightarrow{\gamma^{-1}} & g \end{array} \tag{8}$$

Note that if γ tends to an affine transformation, *i.e.* $\mu \to 0$ implying $\gamma(v) = \alpha + \beta v$, one reobtains the linear equation. This is as one would expect, since the affine group is in fact precisely the invariance group of Eq. (3) under grey-scale point mappings.

One might conjecture that Eq. (5) is no longer invariant under affine grey-scale transformations. However, one should not fail to notice that the parameter μ and the image v are dimensionally dependent, so that the affine group also affects μ. Indeed, $(v; \mu) \to (\alpha + \beta v; \mu/\beta)$ with $\beta \neq 0$ is the full invariance group corresponding to affine grey-scalings in the new representation defined by Eq. (4).

In order to cope with the nonlinear schemes one may exploit the commuting diagram of Eq. (8).

Proposition 1. *Let* $\star$ *denote correlation, i.e.*

$$f \star \phi(x) \stackrel{\text{def}}{=} \int dz\, f(x+z)\, \phi(z).$$

If ϕ *is the Green's function of Eq.* (3) *then the solution of Eq.* (5) *is given by*

$$v \stackrel{\text{def}}{=} \gamma^{-1}(\gamma(g) \star \phi).$$

Recall that the Green's function of Eq. (3) is the normalised Gaussian,

$$\phi(z; \sigma) \stackrel{\text{def}}{=} \frac{1}{\sqrt{2\pi\sigma^2}^n} \exp\left(-\frac{1}{2}\frac{\|z\|^2}{\sigma^2}\right), \tag{9}$$

in which the inner scale parameter σ is related to the evolution parameter s of Eq. (3) by $\sigma = \sqrt{2s}$.

We henceforth assume that the initial image f is normalised to the unit interval, and that $\gamma : [0, 1] \to [0, 1]$ preserves this range. It is then easily seen that confinement to the unit interval is preserved under evolution by Eq. (5).

The fact that Eq. (5) is a generalisation of linear scale-space defined in terms of an infinite-dimensional function space adds more flexibility to the way Gaussian scale-space theory can be used in practical applications. As opposed to general nonlinear diffusion schemes all rigorous results known for the linear case still hold in some precise form. We discuss a number of concrete possibilities below.

2.1. *Scalar Images*

We first consider the case in which we are given a single image, and discuss the relevance of the theory for image processing, front-end vision, image analysis, and edge detection.

2.1.1. Image Processing. Recall Eqs. (5–8). Of all possible non-affine transformations, one class is particularly simple and somewhat special, viz. the one for which the coefficient μ is a global constant. A particular case arises in the limits $\mu \to \pm\infty$. A perturbative approach reveals that one then obtains first order evolution equations, which can be regarded as the morphological counterparts of Eq. (3):

$$\begin{cases} \partial_t v = \pm\|\nabla v\|^2, \\ \lim\limits_{t\to 0} v = g. \end{cases} \tag{10}$$

See e.g. Boomgaard et al. [2–5] and Dorst et al. [6] for details. We will return to these limiting cases below.

The general case is of interest in the development of generalised multiscale techniques beyond the standard linear and morphological methods based on Eqs. (3) and (10), respectively [8]. More specifically, it is interesting for its potential role in finding a balance between these extremal cases that brings out the best of two worlds. For instance, the linear theory is appreciated for its robustness due to its regularising property (cf. Nielsen et al. [20]), whereas the morphological theory is often preferred in cases where discontinuities are considered essential.

The transformation corresponding to finite constant μ depends on the choice of two integration constants and is given by the following lemma.

Lemma 1. *Consider the parametrised transformation* $u = \gamma_\mu(v)$ *given by*

$$\gamma_\mu(v) = \begin{cases} \beta \dfrac{e^{\mu v} - 1}{\mu} + \alpha & \text{if} \quad \mu \neq 0, \\ \beta v + \alpha & \text{if} \quad \mu = 0. \end{cases}$$

This transforms Eq. (3) *into Eqs.* (5–6) *with a constant coefficient* $\mu \in \mathbb{R}$. *Apart from* μ *there are two degrees of freedom in the transformation,* $\alpha \in \mathbb{R}$ *and* $\beta \in \mathbb{R}^+$.

Note that the constants $\alpha = \gamma_\mu(0)$ and $\beta = \gamma'_\mu(0)$ are actually independent of μ. There is no loss of generality in the discussion that follows if we fix suitable values for α and β. It is, however, more realistic to restrict image values to the unit interval, and to maintain this range regardless of the mapping, because raw images always have a finite range. This boils down to a combination of suitable integration constants that *does* depend on μ, viz. $\alpha = 0$ and $\beta = \mu/(e^\mu - 1)$ if $\mu \neq 0$, $\beta = 1$ otherwise. This observation has significant implications for the morphological limits, as will be seen later.

Definition 1. By means of a suitable affine transformation we henceforth restrict the isomorphism of Lemma 1 to the unit interval: $\gamma_\mu(0) \equiv 0$ and $\gamma_\mu(1) \equiv 1$. That is,

$$\gamma_\mu(v) = \begin{cases} \dfrac{e^{\mu v} - 1}{e^\mu - 1} & \text{if} \quad \mu \neq 0, \\ v & \text{if} \quad \mu = 0. \end{cases}$$

As a consequence of this definition all image quantities, f, g, u and v, as well as the parameter μ appear dimensionless. It is not difficult to reintroduce appropriate units if desired. We have

$$\gamma_\mu^{-1}(u) = \begin{cases} \dfrac{1}{\mu} \ln(1 + (e^\mu - 1)u) & \text{if } \mu \neq 0, \\ u & \text{if } \mu = 0. \end{cases} \tag{11}$$

Both γ_μ as well as γ_μ^{-1} are continuously differentiable for all $\mu \in \mathbb{R}$, in other words, the isomorphism is even a *diffeomorphism*. This observation may be important in view of techniques or proofs that exploit the commuting diagram of Eq. (8).

We have the following limiting cases (χ_I is the indicator function on I, i.e. $\chi_I(x) = 1$ if $x \in I$, otherwise $\chi_I(x) = 0$; $[a, b[$ denotes the half-open interval including a but excluding b, etc.) :

$$\lim_{\mu \to +\infty} \gamma_\mu(v) = 1 - \chi_{[0,1[}(v), \tag{12}$$

$$\lim_{\mu \to +\infty} \gamma_\mu^{-1}(u) = \chi_{]0,1]}(u), \tag{13}$$

respectively

$$\lim_{\mu \to -\infty} \gamma_\mu(v) = \chi_{]0,1]}(v), \tag{14}$$

$$\lim_{\mu \to -\infty} \gamma_\mu^{-1}(u) = 1 - \chi_{[0,1[}(u). \tag{15}$$

Convergence is pointwise, not uniform. In particular one observes that the limiting pairs are no longer each other's inverse and fail to be isomorphisms.

Combination of Eq. (9) and Definition 1 leads us to consider

$$v_\mu(x; \sigma) = \frac{1}{\mu} \ln \int dz\, e^{\mu g(x+z)}\, \phi(z; \sigma)\,, \tag{16}$$

in which the *inner scale parameter* σ is related to the evolution parameter s of Eq. (3) by $\sigma = \sqrt{2s}$. For every $\mu \in \mathbb{R}$ this formula gives us the explicit nonlinear filtering procedure for obtaining a particular multiscale representation of the raw image g corresponding to a member of a 1-parameter family of pseudo-linear scale-spaces governed by the control parameter μ. The integral is always well-defined by virtue of the normalisation of grey-values: $0 \leq g(z) \leq 1$ for all z. It is easily seen that confinement to the unit interval is preserved at all scales and for all parameter values.

Let us return to the aforementioned limiting cases.

Proposition 2 (*Linear Scale-Space*)**.** *Recall Eqs.* (9) *and* (16)*. The limit*

$$u \stackrel{\text{def}}{=} \lim_{\mu \to 0} v_\mu$$

exists and reproduces linear scale-space filtering:

$$u(x; \sigma) = \int dz\, g(x + z)\, \phi(z; \sigma).$$

Convergence is uniform.

According to Eq. (7) and Definition 1 we can identify $g = f$.

Proof: Observe that $v_\mu = g \star \phi + \mathcal{O}(\mu)$ as $\mu \to 0$, with $g = f + \mathcal{O}(\mu)$. □

It will turn out that for nonzero parameter μ a scale different from "linear scale" σ will show up in the analysis.

Proposition 3 (*Morphological Scale-Spaces*)**.** *Recall Eqs.* (9) *and* (16)*. For given linear scale* $\sigma \in \mathbb{R}^+$ *and nonlinearity parameter* $\mu \in \mathbb{R}$ *we define the "nonlinear scale" parameter* $\tau \in \mathbb{R}^+$ *as follows*:

$$\tau \stackrel{\text{def}}{=} \sigma\sqrt{|\mu|},$$

and consider $u_\mu(x;\tau) \equiv v_\mu(x;\sigma)$*. Keeping* τ *fixed, the limits*

$$u_{\pm\infty} \stackrel{\text{def}}{=} \lim_{\mu\to\pm\infty} u_\mu$$

exist and are given by

$$u_{+\infty}(x;\tau) = \sup_{z\in\mathbb{R}^n}[g(x+z) + q_+(z;\tau)],$$
$$u_{-\infty}(x;\tau) = \inf_{z\in\mathbb{R}^n}[g(x+z) + q_-(z;\tau)],$$

with

$$q_\pm(z;\tau) \stackrel{\text{def}}{=} \mp\frac{1}{2}\frac{\|z\|^2}{\tau^2}.$$

Convergence is pointwise.

Note that in these limiting cases we can no longer use Eq. (7) Definition 1 to relate the initial images f and g. In mathematical morphology the functions $u_{+\infty}$ and $u_{-\infty}$ obtained according to this recipe are known as the *dilation*, respectively the *erosion of g by* $q = q_+$. The function q is known as the *quadratic* or *parabolic structuring function* [2–6, 16, 23], which, by the recipe of Proposition 3, induces a multiscale representation of g known as the *dilation*, respectively *erosion scale-space*, with "morphological scale" τ.

Proof: The idea is to keep τ fixed in a physical representation:

$$u_\mu(x;\tau) \stackrel{\text{def}}{=} \frac{1}{\mu}\ln\left\{\int dz\, e^{\mu g(x+z)}\phi(z;\sigma)\right\},$$

in which it is understood that $\sigma = \tau/\sqrt{|\mu|}$. To this end we rewrite the r.h.s.—using the explicit formula for the normalised Gaussian, Eq. (9), and writing $\hat{\mu}$ for the sign of μ—as

$$\frac{1}{\mu}\ln\left\{\sqrt{|\mu|}^n\int dz\, e^{\mu[g(x+z)+q_{\hat{\mu}}(z;\tau)]}\right\}$$
$$= \frac{1}{\mu}\ln\int dz\, e^{\mu[g(x+z)+q_{\hat{\mu}}(z;\tau)]} + \mathcal{O}\left(\frac{\ln|\mu|}{\mu}\right)$$

as $\mu \to \pm\infty$. The latter term vanishes in either limit, and the result follows from the standard formulas (using continuity and monotonicity of the logarithm)

$$\lim_{\mu\to+\infty}\left\{\int dz\,\varphi^\mu(z)\right\}^{\frac{1}{\mu}} = \sup_{z\in\Omega}\varphi(z),$$
$$\lim_{\mu\to-\infty}\left\{\int dz\varphi^\mu(z)\right\}^{\frac{1}{\mu}} = \inf_{z\in\Omega}\varphi(z),$$

which hold for positive and bounded $\varphi \in C(\Omega) \cap L^1(\Omega)$ with support Ω. □

The proof brings out the significance of the rescaling introduced in Proposition 3. In terms of the evolution parameters of corresponding initial value problems we have a rescaling $t = |\mu|\, s$, in which $2s = \sigma^2$, $2t = \tau^2$ (*modulo* offset determined by the initial scale of the data). If we apply this to Eq. (5) we obtain

$$\begin{cases} \partial_t u_\mu = \dfrac{1}{|\mu|}(\Delta u_\mu + \mu\,\|\nabla u_\mu\|^2), \\ \lim\limits_{t\to 0} u_\mu = g, \end{cases} \tag{17}$$

which indeed reproduces both Eq. (3) as well as Eq. (10) in the respective limits, but at the same time shows that the associated scale parameters are related in a nontrivial way, viz. by a *renormalisation*, *i.e.* an "infinite rescaling". The ultimate justification for such an awkward procedure is the law of *scale invariance* (cf. the "Pi Theorem" [21]). This implies that entities existing at *whatever* (finite) morphological scale pertain to structures in the input image *at infinite spatial resolution, regardless of their measure*. This introduces a hyper-sensitivity which obviously poses problems if data are not carefully prepared or preprocessed (think of "noise spikes" that are negligible in L^1-norm yet of appreciable size in L^∞-norm).

Renormalisation also implies that we cannot compare linear and morphological scale-spaces on a slice-by-slice basis along scale axes. One is compelled to maintain the distinction between morphological scale on the one hand—scale in the sense of the

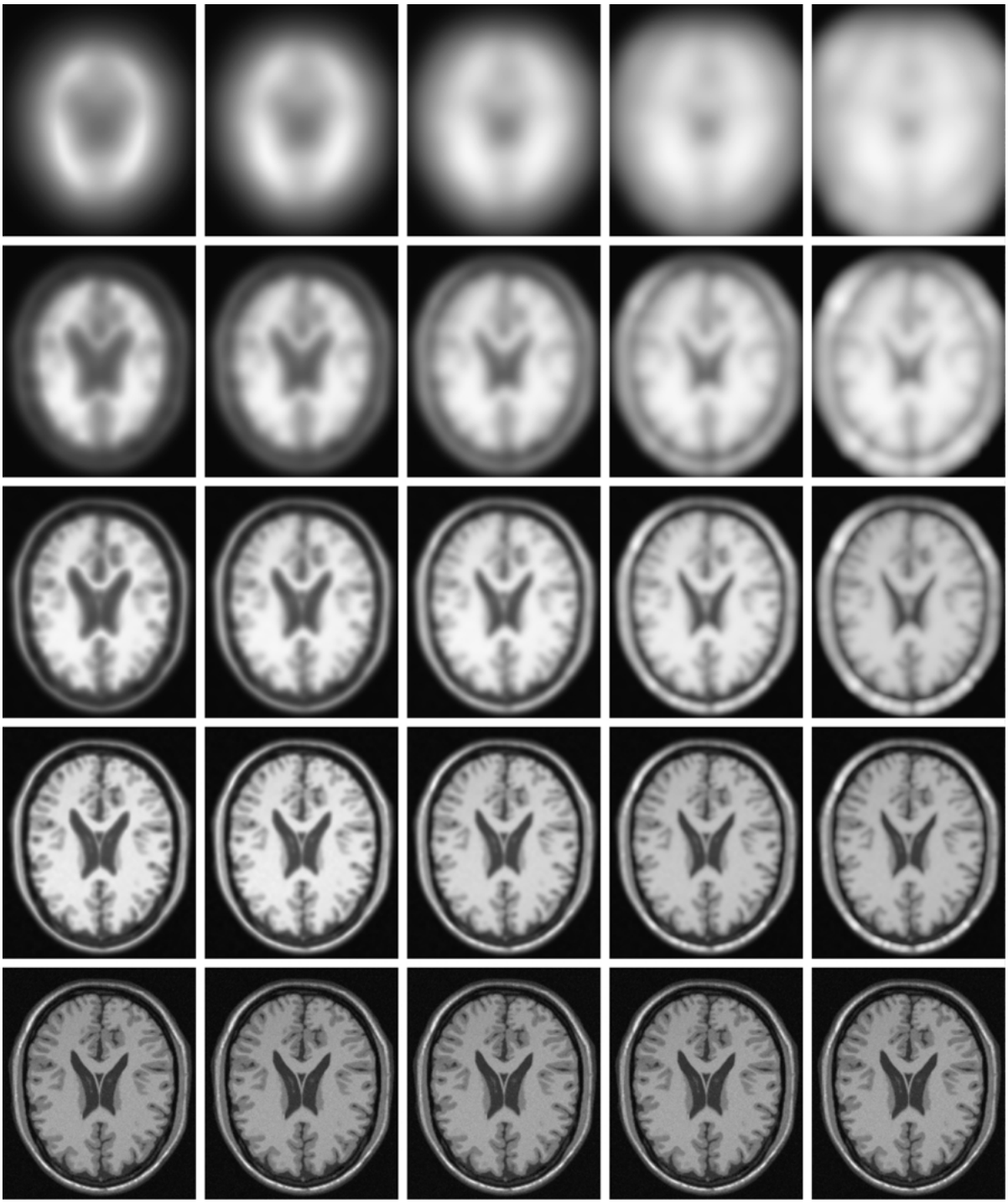

Figure 1. Pseudo-linear scale-space representations of MRI image, obtained according to Eqs. (5–7) for constant μ. Scale $\sigma = \sqrt{2s}$ varies exponentially in vertical direction: $\sigma = 2^k$ pixels, with $k = 0, 1, 2, 3$ (bottom up). The parameter μ varies in horizontal direction: from left to right we have $\mu = -8, -4, 0, 4, 8$, respectively. Dark regions are pronounced in erosion-like schemes ($\mu < 0$) whereas bright regions are emphasised in dilation-like schemes ($\mu > 0$).

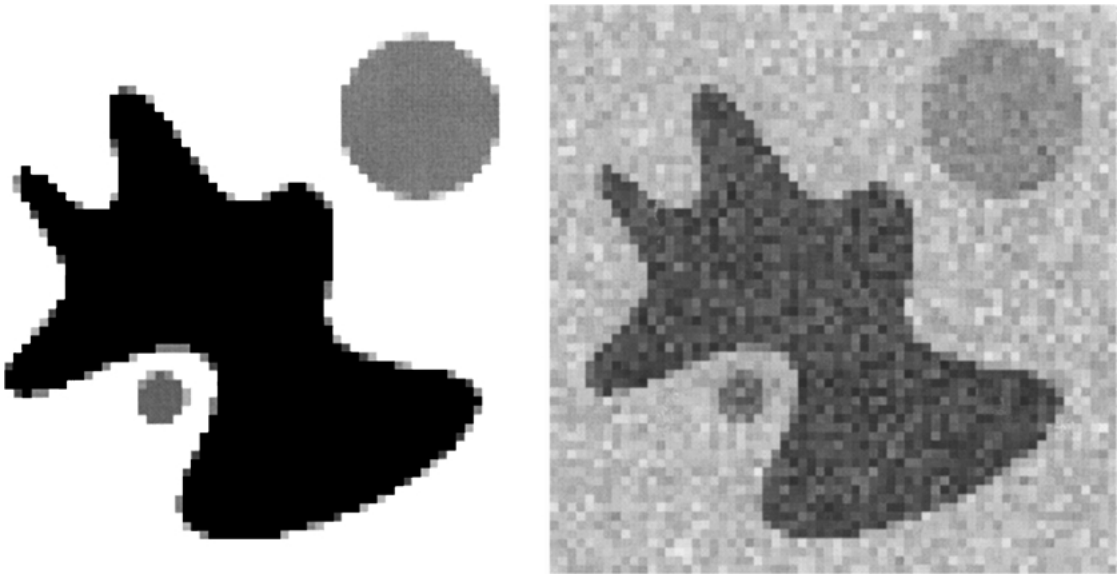

Figure 2. Image used in the comparison of pseudo-linear scale-spaces. Left: synthetic image showing a few blobs, 64×64 pixels, 1 byte per pixel. Right: same image perturbed with additive pixel-uncorrelated Gaussian noise with variance 1000, i.e. a standard deviation equal to 12.4% of the global intensity maximum (255). This perturbed image is the one actually used in the computations.

renormalised parameter τ—*versus* linear scale σ on the other. Scales can no longer be synchronised as opposed to the pseudo-linear case.

According to previous observations, the following definition of a pseudo-linear scale-space representation appears to be the natural one.

Definition 2. Recall Eqs. (9) and (16). For every $\mu \in \mathbb{R}\backslash\{0\}$ we define the *pseudo-linear scale-space*

$$u_\mu(x;\tau) = \frac{1}{\mu} \ln \int dz\, e^{\mu g(x+z)}\, \phi(z;\tau/\sqrt{|\mu|}).$$

In this formulation linear and pseudo-linear scales have been synchronised according to Proposition 3.

By slick choice of units, starting out from any intermediate value $\mu \neq 0, \pm\infty$, we can always replace an isolated member of the μ-family by one of two canonical forms:

$$u_{\pm 1}(x;\tau) = \pm \ln \int dz\, e^{\pm g(x+z)}\, \phi(z;\tau). \qquad (18)$$

However, in practice one will need some operational criterion for tuning the nonlinearity, based on a physical interpretation of μ [8].

Figure 1 illustrates the pseudo-linear scale-spaces one obtains for finite values of μ. To highlight the effect on topology, we consider the synthetic image shown in Fig. 2. Figure 3 shows contourplots of *corresponding* slices from pseudo-linear scale-space representations obtained for this input image for several values of the parameter μ.

Correspondence entails the existence of an isomorphism, which has been shown to require a definite coupling of "linear" and "pseudo-linear scales" according to $\tau = \sigma\sqrt{|\mu|}$. In Fig. 3 we have kept σ fixed. One may observe that although grey-value tags of iso-contours are mapped by the isomorphism, their geometry is left unaffected, as expected. Note also that positive values of μ encourage grey-level segregation in dark regions, whereas negative values show the opposite tenet. This bias is a familiar phenomenon in the limiting dilation and erosion schemes, and can be exploited in practical applications such as object segmentation if specific priors on the histogram are available (e.g. knowledge of signal production caused by specific tissues in medical imaging, blood dyeing in Digital Subtraction Angiography, histological colouring in microscopy, etc.).

Correspondence in the strict sense of isomorphism ceases to hold in the morphological limits $\mu \to \pm\infty$, but a formal correspondence with the linear theory

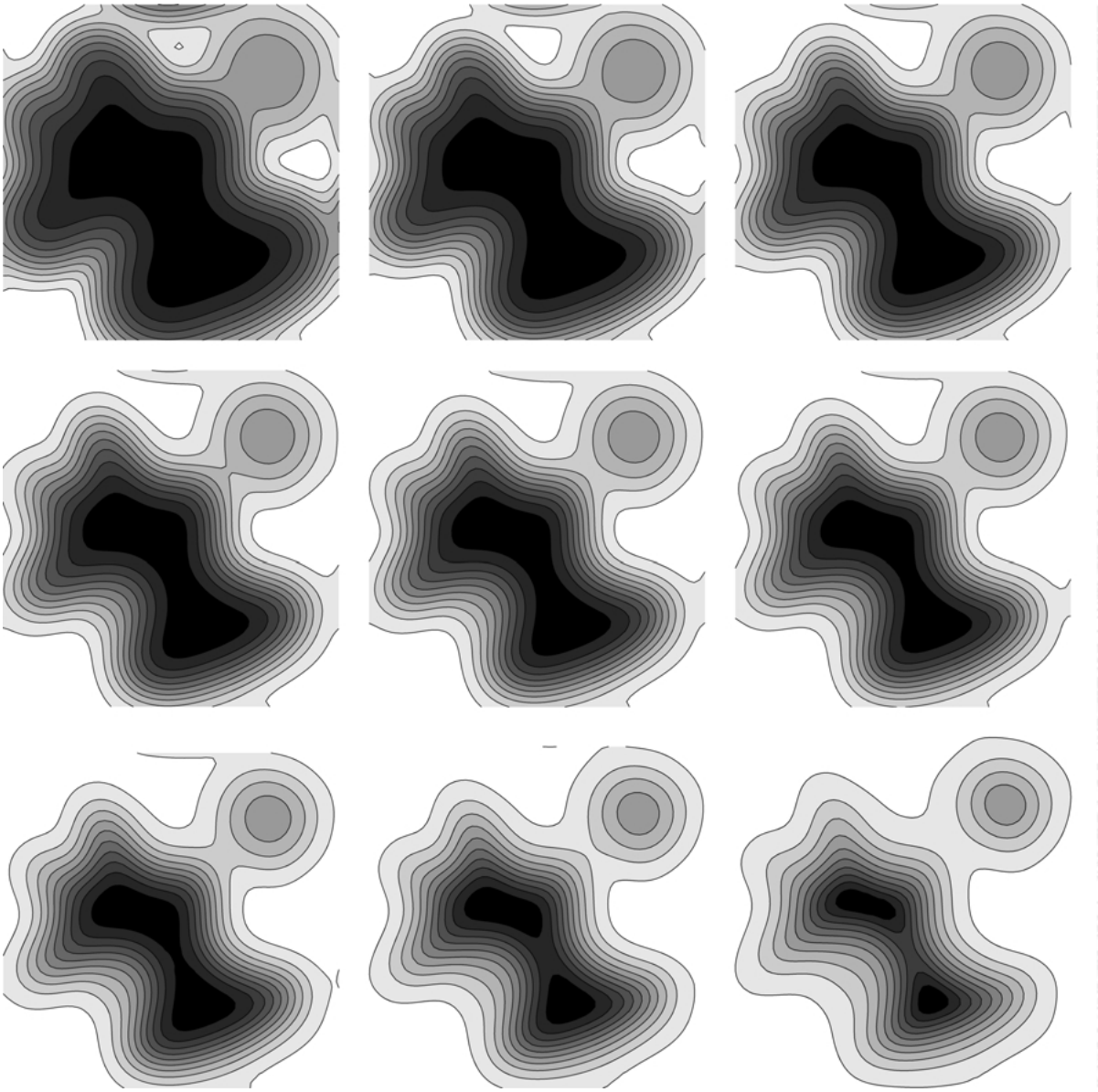

Figure 3. Pseudo-linear scale-space images all evaluated at fixed isotropic "linear scale" $\sigma = 4$ pixels. From top left to bottom right we have parameter values $\mu = -8, -4, -2, -1, 0, 1, 2, 4, 8$, respectively, corresponding to "pseudo-linear" scales $\tau = 11.3, 8.0, 5.7, 4.0, 0.0, 4.0, 5.7, 8.0, 11.3$ pixels, cf. the definition of τ in Proposition 3. The computation confirms that these scale-slices indeed appear isomorphic; the iso-contours have the same geometry in all images.

via renormalisation or suitable limiting procedures—and consequently the analogies implied by this[1]—is maintained as explained in the previous section. This means that certain axioms that hold in the linear/morphological domain will continue to hold in the morphological/linear limits, viz. those that do not rely on uniform convergence.

Figure 4 illustrates that if one keeps τ fixed, in this case $\tau = 4$ pixels, one indeed obtains image representations that differ topologically for different values of μ. For larger $|\mu|$ one observes higher resolution details, again as expected.

For large parameter values we may interpret the pseudo-linear scale-space representation as a *fuzzy*

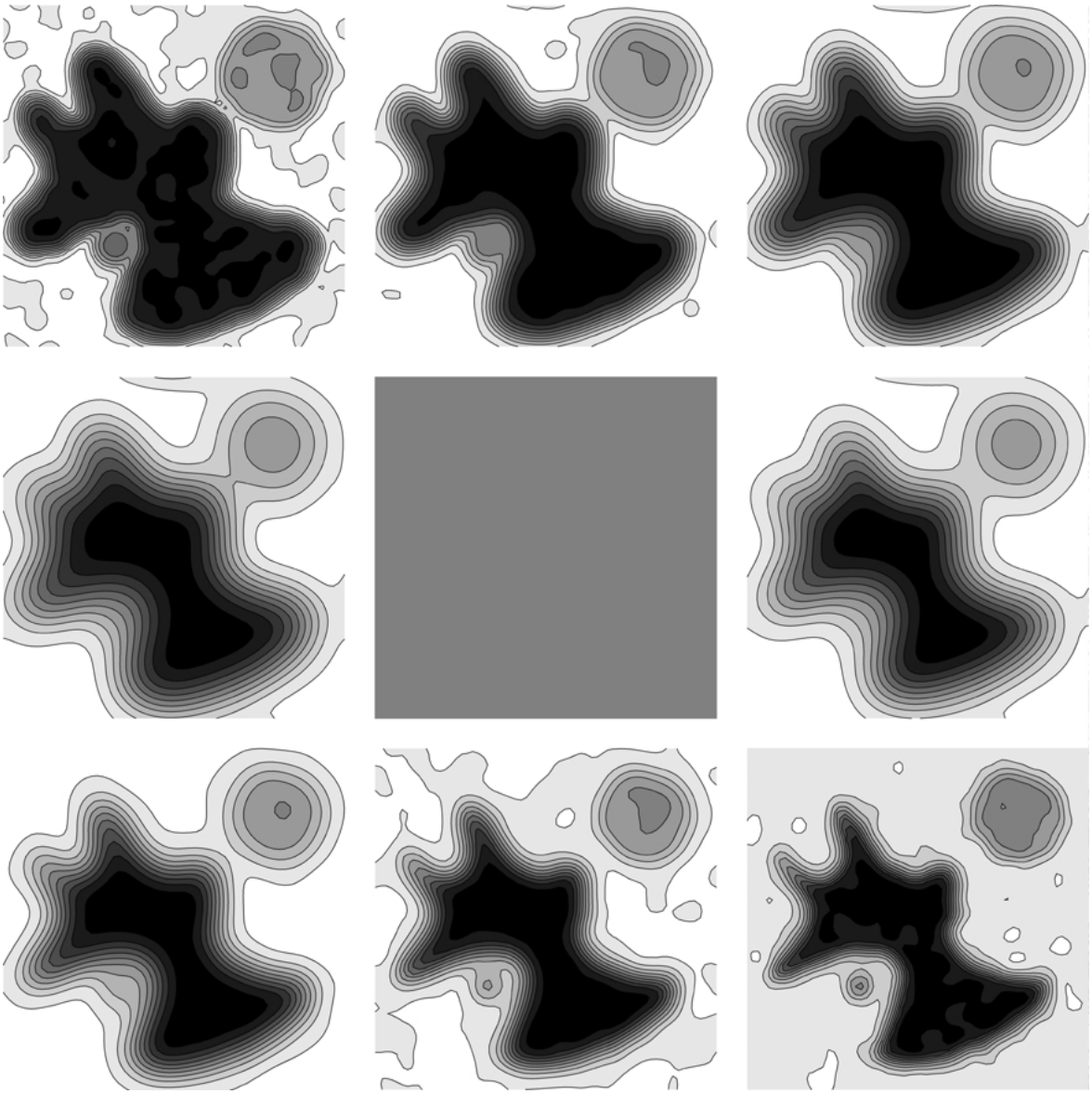

Figure 4. Pseudo-linear scale-space images all evaluated at fixed isotropic "pseudo-linear" scale $\tau = 4$ pixels. From top left to bottom right we have parameter values $\mu = -8, -4, -2, -1, 0, 1, 2, 4, 8$, respectively, corresponding to "linear scales" $\sigma = 1.4, 2.0, 2.8, 4.0, \infty$, 4.0, 2.8, 2.0, 1.4 pixels, cf. the definition of τ in Proposition 3. The degenerate case in the middle corresponds to zero resolution, i.e. to an overall grey-scale averaging. These scale-slices are clearly *not* isomorphic.

dilation ($\mu \gg 0$), respectively a *fuzzy erosion* ($\mu \ll 0$) by the quadratic structuring element $q(z; \tau)$. This should, however, not be confused with the definition of fuzziness proposed by Bloch and Maître [1]. Their goal was to provide a generic framework capturing various existing fuzzy methods in mathematical morphology, while insisting on certain basic demands that hold for the classical, i.e. non-fuzzy case. One such basic demand is *idempotency*, which explains their use of sup and inf operators (in addition to a "triangular norm"). However, idempotency does not hold in the (general) case of linear processing, nor in the pseudo-linear theory presented here, except trivially for the morphological limits. Rather, our notion of fuzziness pertains

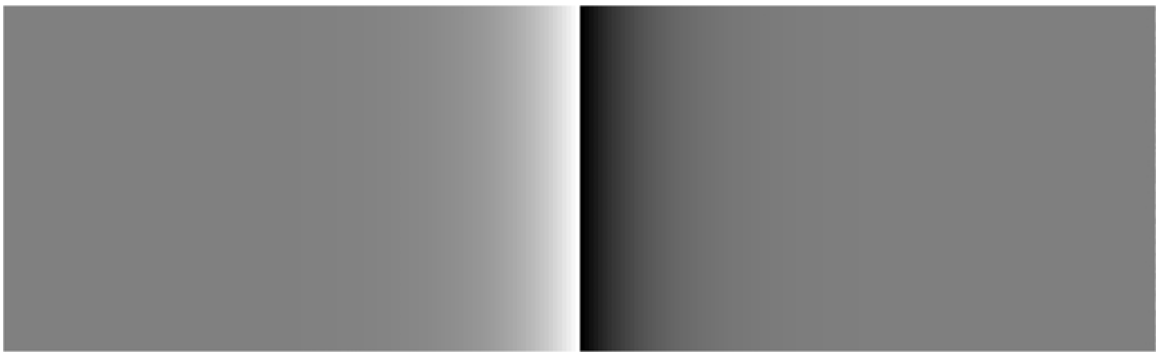

Figure 5. Craik–O'Brien–Cornsweet illusion: The region $x \ll 0$ appears brighter than the region $x \gg 0$ ($x = 0$ is in the middle). Both have equal grey-tone, however; the effect is induced by the profile of the transient layer $x \approx 0$, which becomes apparent by covering it with your finger.

to the compromise between classical, non-fuzzy mathematical morphology (based on the quadratic structuring function) and intrinsically fuzzy, linear processing. In view of the constructed isomorphism it remains an intriguing question whether both types of fuzziness could be joined into a single concept by, say, relaxing the condition of idempotency, and possibly introducing other fundamental demands that do not exclude the linear case from the outset.

2.1.2. Front-End Vision. Apart from the fact that Eqs. (5–7) and Lemma 1 yield scale-spaces that are in some precise sense "in-between" the familiar linear and morphological ones, which is of interest in its own right, they may also provide a valuable model for front-end visual processing, as they account for a logarithmic compression of the raw input distribution f (the photon flux impinging onto the retina), as well as for multiple scales. Note that, for instance, Weber's and Fechner's laws [10] arise naturally for values of u that are well above threshold. For suppose that $\mu \gg 0$, then a least noticeable perceptual difference dv corresponds to a logarithmic increment $\mu^{-1}\, du/u$ of photon flux. One could interpret $v_0 = \mu^{-1}$ as a psychophysical unit of dimension for the quantity v. The constant u_0 may be adaptive to ambient light conditions to the extent that the potentially available range of v-values (neural firing patterns in-between threshold and saturation frequencies) is actually realized for a steady stimulus. For $\mu \approx 0$ we find a linear correspondence $dv = du$ instead.

The Weber–Fechner law holds only within an interval of physical photon fluxes of a few orders of magnitude. Threshold and saturation phenomena can, however, be accounted for by the same token, in which case the mapping γ is still one-to-one (for each distinguishable perceptual brightness level there is a unique physical irradiance), but no longer onto (irradiances beyond threshold and saturation cannot be segregated). A way to achieve this is to replace the unbounded mapping γ above by $\gamma_\chi = \gamma \circ \chi$ for some suitably chosen psychophysical function χ, such that χ^{inv} is bounded and monotonic, say $\chi^{\text{inv}} : \mathbb{R} \to (0, 1)$. This amounts to a replacement of the nonlinearity coefficient $\mu \to \mu_\chi = \mu\chi' + \chi''/\chi'$.

Isomorphism between retinal irradiance and perceived brightness is of course merely an idealisation that holds only within certain physical limits and if lateral interactions can be ignored. An example of significant lateral interaction arises in the so-called Craik–O'Brien–Cornsweet illusion; adjacent regions of identical luminance separated by a narrow region with a particular transient luminance profile induce distinct brightness percepts: Fig. 5.

2.1.3. Image Analysis. The general case, Eqs. (5–7), is of interest in the development of specialised multiscale techniques. More specifically, since the mapping introduces a particular bias in the grey-value domain, it is interesting for its potential role in accounting for a priori knowledge that warrants such a bias.

One way to obtain a monotonic mapping is as follows:

$$\gamma(v) = \int_0^v dy\, \varrho(y), \tag{19}$$

in which $\varrho(y)$ is some positive measure, normalised such that $\gamma(1) = 1$ (say). This measure could be the image's grey-value histogram, or any other histogram inspired by some tissue/image model (v.i.). However,

one should be a bit careful and take into account that error propagation is governed by the Jacobian of the mapping, i.e. $\gamma'(v) = \varrho(v)$, so that an error δu in the u-domain corresponds to an error $\delta v = \delta u/\varrho(v)$ in the v-domain. If for some values of v the measure $\varrho(v)$ is nearly zero this obviously becomes problematic. A hack around this problem could be to replace $\varrho(y)$, if it is problematic, by $\varrho_\varepsilon(y) = \varrho(y) + \varepsilon$, for some $0 < \varepsilon \ll 1$ (of course one should then renormalise $\varrho_\varepsilon(y)$ again to unit weight). This guarantees that the Jacobian always exceeds ε, thus tempering the errors. A similar effect is obtained if one restricts grey-values to a subinterval in which $\varrho(y) > \varepsilon$ (although one may then loose information it may not be a problem depending on one's task, e.g. segmentation of one particular tissue type in medical imaging). A similar regularisation effect could be obtained by blurring the measure $\varrho(y)$ in the y-domain [15]. A natural scale for this could be the quantisation error of the initial image or the noise amplitude in the case of additive noise. Perhaps a better way to avoid problems is to simply remain cautious and take error propagation into account throughout the analysis.

Applying Eqs. (6–19) one obtains a nonlinearity coefficient that is given by

$$\mu = (\ln \varrho)'. \tag{20}$$

From this we see that at critical points of the histogram measure, i.e. if $\varrho' = 0$ (assuming $\varrho \neq 0$), the nonlinearity coefficient vanishes and the blurring becomes linear. On the other hand, if $\varrho = 0$ (while $\varrho' \neq 0$), the nonlinearity coefficient becomes degenerate.

A possible way of exploiting Eq. (20) is to enhance image evidence for a particular tissue type of which the a priori histogram is known. If the appropriate modality is used such a histogram is typically unimodular, so that Eq. (19) will indeed produce an invertible mapping within a subinterval of grey-values. Of course the bias introduced by the mapping will also enhance other tissue types insofar as their grey-value histograms overlap with that of the desired one. See Fig. 6.

2.1.4. Edge Detection. By virtue of the nonlinearity degree of freedom, the pseudo-linear Laplacean on the r.h.s. of Eq. (5) may be of some interest in itself as an adaptable edge detector akin to the classical one proposed by Marr and Hildreth [18]. Note that it is important to account for the dimensional discrepancy between Δv and $\|\nabla v\|^2$, in other words, for the fact

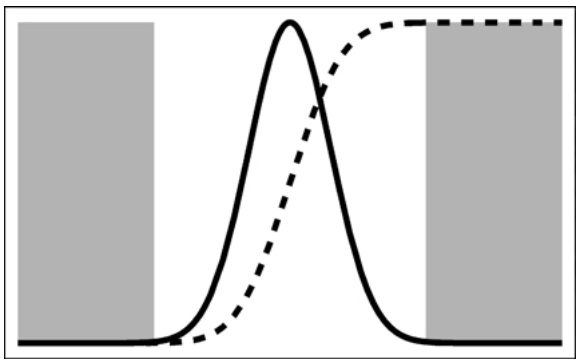

Figure 6. The prior distribution $\varrho(v)$ of grey-values (solid curve) induced by a particular tissue type is usually unimodular, at least for bulk material. Its primitive $\gamma(v)$ (dashed curve) is consequently strictly monotonic within the grey-value interval of interest (i.e. in-between the shaded regions), and may therefore serve as an admissible transformation. Information pertaining to the shaded regions is lost, while uncertainty increases towards the boundaries.

that μ is actually a dimensionful parameter. In this case we normalise the image to the unit interval (as before) prior to edge detection. In fact, one *ought to* consider the general form $\Delta v + \mu\|\nabla v\|^2$ instead of Δv as this *is* the image's Laplacean in case one is in lack of additional knowledge or some explicit hypothesis on grey-scale parametrisation that warrants the assumption that $\mu = 0$. If no such knowledge or hypothesis is available one should consider μ as an essentially undetermined function of the image v, recall Eq. (6).

As a particular case, it is relevant to consider the behaviour of the pseudo-linear Laplacean when used as an edge detector as a function of μ (taken to be a constant real number). Figures 7–8 illustrate the behaviour of the zero-crossings defined by $\Delta v + \mu\|\nabla v\|^2 = 0$ as μ is varied.

Note that for all ϵ with $0 < \epsilon \ll 1$ there exists a sufficiently large parameter threshold $M > 0$ such that for $\mu > M$ $(\mu < -M)$, the total volume enclosed by all (closed) zero-crossing contours does not exceed ϵ. The only zero-crossings surviving the limit $M \to \infty$ are sets of measure zero satisfying $\nabla v =$ and $\Delta v = 0$. Thus at almost all scales σ the zero-crossings will eventually vanish as one increases (decreases) the value of μ, the only residuals being isolated critical points in scale-space.

2.2. Multi-Component Images

Next we consider a possible extension to deal with multi-component images. One has to distinguish

Figure 7. Eye region of "Lena" image, size 84×74 pixels.

between vector-valued images and multispectral images (which may not be part of a vector, i.e. linear space).

2.2.1. Vector-Valued Images. Suppose we have a vector-valued raw image $\mathbf{g}(x)$ with components $g^\mu(x)$ relative to a coordinate basis, i.e.[2] $\mathbf{g}(x) = g^\mu(x)\mathbf{e}_\mu$, for which we would like to define a scale-space extension $\mathbf{v}(x;s) = v^\mu(x;s)\mathbf{e}_\mu$. Let us furthermore assume that u is some scalar field obtained from $\mathbf{v}$, e.g. the scalar product $\mathbf{v}\cdot\mathbf{v}$. Since this is a scalar it is not unreasonable to require that it satisfies the linear diffusion equation, Eq. (3), although any other scalar that can be constructed from $\mathbf{v}$ would be an equally legitimate choice (i.e. any power of the scalar product, such as the magnitude $\|\mathbf{v}\|$). For reasons of generality let us assume that the scalar of interest is given by

$$u = \gamma(\mathbf{v}). \tag{21}$$

By substitution into Eq. (3) one then finds that the components of $\mathbf{v}$ must satisfy

$$\gamma_\mu \partial_s v^\mu = \gamma_\mu \Delta v^\mu + \gamma_{\nu\rho}\nabla_\alpha v^\nu \nabla^\alpha v^\rho, \tag{22}$$

in which γ_μ and $\gamma_{\nu\rho}$ are first and second order derivatives of γ. If the Jacobian has maximal rank we can use the γ_μ, $\mu = 1,\ldots,n$, as a basis, and we can write

$$\gamma_{\nu\rho} = \mu^\mu_{\nu\rho}\gamma_\mu, \tag{23}$$

for some $(n+1)$-tensor with components $\mu^\mu_{\nu\rho}(\mathbf{v})$. Substituting this into Eq. (22) we then obtain

$$\begin{cases} \partial_s v^\mu = \Delta v^\mu + \mu^\mu_{\nu\rho}\nabla_\alpha v^\nu \nabla^\alpha v^\rho \\ \lim\limits_{s\to 0} v^\mu = g^\mu. \end{cases} \tag{24}$$

which prescribes the scale-space representation for the individual components g^μ of the raw vector field $\mathbf{g}$, consistent with the linear representation of Eq. (3) for the scalar $f = \gamma(\mathbf{g})$. Eqs. (23–24) are the vector analogues of Eqs. (5–6), with the scalar nonlinearity $\mu(v)$ replaced by the nonlinearity tensor $\mu^\mu_{\nu\rho}(\mathbf{v})$.

As an example, suppose $u = \gamma(\mathbf{v}) = \sqrt{\mathbf{v}\cdot\mathbf{v}}$, i.e. we take the magnitude of the vector field as the scalar that we wish to subject to a linear scale-space representation. In this case the components of the nonlinearity tensor are given by

$$\mu^\mu_{\nu\rho}(\mathbf{v}) = \frac{1}{\|\mathbf{v}\|^2}\left(\eta_{\nu\rho}\delta^\mu_\sigma - \frac{1}{2}\left(\eta_{\nu\sigma}\delta^\mu_\rho + \eta_{\rho\sigma}\delta^\mu_\nu\right)\right)v^\sigma, \tag{25}$$

in which $\eta_{\mu\nu}$ are the components of the Euclidean metric tensor (in a Cartesian coordinate system equal to 1 if and only if $\mu = \nu$, otherwise 0), and δ^ν_μ are the invariant components of the Kronecker tensor (similarly defined in an arbitrary coordinate system). It should be noted that the tensor is completely parameter free.

Example 1. Consider a 2D vector field $\mathbf{v} = (v, w)$, e.g. a multiscale motion field. If the components are subject to the following system of coupled nonlinear diffusion equations,

$$\begin{cases} \partial_s v &= \Delta v - \dfrac{1}{v^2+w^2}(w\nabla v - v\nabla w)\cdot\nabla w \\ \partial_s w &= \Delta w - \dfrac{1}{v^2+w^2}(v\nabla w - w\nabla v)\cdot\nabla v, \end{cases}$$

then the magnitude image $u = \|\mathbf{v}\| = \sqrt{v^2+w^2}$ satisfies the linear scale-space equation, Eq. (3).

Note that the denominator on the right hand side of Eq. (25) or Example 1 is strictly positive if the high resolution vector image is not globally zero, since its square root satisfies the isotropic linear diffusion equation with nonnegative (nonzero) initial condition.

Example 2. If the vector field of Example 1 is a gradient field, $\mathbf{v} = \nabla\psi$ say, then a straightforward computation shows that it satisfies the vector-valued

Figure 8. Pseudo-linear Laplacean zero-crossings, $\Delta v + \mu \|\nabla v\|^2 = 0$, computed for the image shown in Fig. 7. First and second derivatives have been computed as linear scale-space derivatives at an arbitrarily chosen scale $\sigma = 2$ pixels, i.e. by convolution using corresponding derivatives of a normalised Gaussian of width $\sigma = 2$. The original image has been normalised to the unit interval prior to edge detection. From top left to bottom right we have parameter values $\mu = -8, -4, -2, -1, 0, 1, 2, 4, 8$, respectively. Observe how the topology of the zero-crossings changes with μ.

diffusion equation

$$\partial_s \mathbf{v} = (\mathbf{I}\Delta + \mathbf{X})\mathbf{v},$$

in which $\mathbf{I}$ is the 2×2 identity matrix and $\mathbf{X}$ is the matrix defined in terms of the gradient $\mathbf{v} = \nabla\psi$ and Hessian $\mathbf{H} = \nabla\nabla^{\mathrm{T}}\psi$ as follows:

$$\mathbf{X} = \frac{1}{\|\mathbf{v}\|^2}\tilde{\mathbf{H}}\tilde{\mathbf{H}}^{\mathrm{T}},$$

or

$$\mathbf{X} = \frac{1}{\psi_x^2 + \psi_y^2}\begin{pmatrix} \psi_{xy}^2 + \psi_{yy}^2 & -\Delta\psi\psi_{xy} \\ -\Delta\psi\psi_{xy} & \psi_{xx}^2 + \psi_{xy}^2 \end{pmatrix}$$

Here, $\tilde{\mathbf{A}}$ denotes the (transposed) cofactor matrix of (symmetric) $\mathbf{A}$.

2.2.2. Multispectral Images. Now suppose we have a collection of multispectral images $g_\alpha, \alpha = 1, \ldots, N$, for which we would like to define a consistent

multiscale representation. Consistency pertains to the presumption that all these images have been obtained by sampling a single source spectrum ϱ according to N different protocols. If we now postulate that Eq. (3) should hold for the unbiased source field

$$u = \int d\lambda\, \varrho(\lambda), \tag{26}$$

then the multiscale representations v_α of g_α must be constrained accordingly.

To be more specific, let us assume that each component v_α is the output of a probing procedure in λ-space that entails two steps: (i) a linear λ-superposition of the spectrum, and (ii) a nonlinear monotonic resampling of the result. That is, if γ_α is the inverse of the latter resampling function, then[3]

$$\gamma_\alpha(v_\alpha) = \int d\lambda \varrho_\alpha(\lambda). \tag{27}$$

It is convenient to introduce the efficiency function η_α for channel α, which takes values in the unit interval and together with the other channels constitutes a partition of unity:

$$\varrho_\alpha(\lambda) = \eta_\alpha(\lambda)\varrho(\lambda) \quad \text{and} \quad \sum_{\alpha=1}^{N} \eta_\alpha(\lambda) = 1. \tag{28}$$

Consequently, the "unbiased" field u is essentially the result of a superposition:

$$\boldsymbol{u} = \gamma(\mathbf{v}) \stackrel{\text{def}}{=} \sum_{\alpha=1}^{N} \gamma_\alpha(v_\alpha), \tag{29}$$

and we can apply the techniques of the previous section. Since the derivative of $\gamma(\mathbf{v})$ with respect to v_α depends only on v_α, the channels are effectively decoupled:

$$\begin{cases} \partial_s v_\alpha &= \Delta v_\alpha + \mu_\alpha \|\nabla v_\alpha\|^2, \\ \lim\limits_{s\to 0} v_\alpha &= g_\alpha\,. \end{cases} \tag{30}$$

in which μ_α corresponds to the only nontrivial component $\mu^\alpha_{\alpha\alpha}$ of the tensor of Eq. (25):

$$\mu_\alpha = \frac{\gamma_\alpha''}{\gamma_\alpha'}, \tag{31}$$

i.e. we have N equations similar to Eqs. (5) and (6) for the scalar case.

To determine the form of the nonlinearity coefficients μ_α one needs to have knowledge of image formation details for the corresponding imaging modalities or protocols, so that one can fill in the missing details of Eqs. (26–29), notably the transfer function γ_α for each channel α.

3. Conclusion

Gaussian scale-space is just the simplest multiscale representation consistent with the scale causality condition that prohibits enhancement of local extrema as scale (resolution) is increased (decreased). Many nonlinear representations exist, which are isomorphic to the linear one ("pseudo-linear scale-spaces"), or related to these by some limiting procedure (morphological scale-spaces).

The theoretical relationship established between linear scale-space based on the Gaussian convolution kernel on the one hand and non-linear, morphological dilation and erosion scale-spaces based on the quadratic structuring function on the other hand is of interest in itself. The pseudo-linear representations, which have been argued to be in a precise sense "in-between" linear and morphological scale-spaces, can be used to balance pros and cons of these well-established limiting cases, and to establish their interconnections.

Pseudo-linear scale-spaces appear to provide the natural multiscale representations in the context of front-end vision, as they potentially account for the non-linearities inherent in retinal mechanisms (Weber–Fechner law). Moreover, they may play an important role in image analysis, as they allow one to introduce grey-scale biases reflecting a priori knowledge of image formation or task. As a particular case it has been argued that the classical Marr–Hildreth Laplacian-of-Gaussian edge detector should be generalised in the absence of such knowledge.

Finally, it has been pointed out that non-linearities are essential when dealing with multi-component images, such as vector-valued or multispectral images. Consistent multiscale representations for the component images have been proposed. Their scale-space properties are still to be investigated.

Notes

1. Deductive proofs are likely to reflect renormalisation in the form of constrained limiting procedures for σ, τ, μ.

2. Summation convention is used throughout: Repeated spatial indices—with values in the range $1, \ldots, n$ in n-dimensional space—are dummies over which a summation is implied.
3. In expressions with only lower indices summation convention does *not* apply.

References

1. I. Bloch and H. Maître, "Fuzzy mathematical morphologies: A comparative study," *Pattern Recognition*, Vol. 28, No. 9, pp. 1341–1387, 1995.
2. R. van den Boomgaard, "Mathematical Morphology: Extensions towards Computer Vision," PhD thesis, University of Amsterdam, March 23 1992.
3. R. van den Bomgaard, "The morphological equivalent of the Gauss convolution," *Nieuw Archief voor Wiskunde*, Vol. 10, No. 3, pp. 219–236, 1992.
4. R. van den Boomgaard and L. Dorst, "The morphological equivalent of the Gaussian scale-space," in Sporring et al. [24], Ch. 15, pp. 203–220.
5. R. van den Boomgaard and A.W.M. Smeulders, "The morphological structure of images, the differential equations of morphological scale-space," *IEEE Transactions on Pattern Analysis and Machine Intelligence*, Vol. 16, No. 11, pp. 1101–1113, 1994.
6. L. Dorst and R. van den Boomgaard, "Morphological signal processing and the slope transform," *Signal Processing*, Vol. 38, pp. 79–98, 1994.
7. L.M.J. Florack, *Image Structure*, Vol. 10 of *Computational Imaging and Vision Series*. Kluwer Academic Publishers: Dordrecht, The Netherlands, 1997.
8. L.M.J. Florack, R. Maas, and W.J. Niessen, "Pseudo-linear scale-space theory," *International Journal of Computer Vision*, Vol. 31, No. 2/3, pp. 247–259, 1999.
9. B.M. ter Haar Romeny, L.M.J. Florack, J.J. Koenderink, and M.A. Viergever (Eds.), in *Scale-Space Theory in Computer Vision: Proceedings of the First International Conference*, Scale-Space'97. Utrecht, The Netherlands, Springer-Verlag: Berlin, July 1997, Vol. 1252 of Lecture Notes in Computer Science.
10. W.R. Hendee and P.N.T. Wells (Eds.), *The Perception of Visual Information*, Springer-Verlag: New York, 1993.
11. T. Iijima, "Basic theory on normalization of a pattern (in case of typical one-dimensional pattern)," *Bulletin of Electrical Laboratory*, Vol. 26, pp. 368–388, 1962 (in Japanese).
12. R. Kimmel and N.A. Sochen, "Geometric-variational approach for color image enhancement and segmentation," in M. Nielsen, P. Johansen, O.F. Olsen, and J. Weickert (Eds.), in *Scale-Space Theories in Computer Vision: Proceedings of the Second International Conference*, Scale-Space'99, Corfu, Greece, pp. 294–305, Berlin, Sept. 1999. Springer-Verlag, Vol. 1682 of Lecture Notes in Computer Science.
13. R. Kimmel, N.A. Sochen, and R. Malladi, "From high energy physics to low level vision," in Haar Romeny et al. [9], pp. 236–247.
14. J.J. Koenderink, "The structure of images," *Biological Cybernetics*, Vol. 50, pp. 363–370, 1984.
15. J.J. Koenderink and A.J. van Doorn, "The structure of locally orderless images," *International Journal of Computer Vision*, Vol. 31, No. 2/3, pp. 159–168, 1999.
16. P.D. Lax, *Hyperbolic Systems of Conservation Laws and the Mathematical Theory of Shock Waves*. SIAM, 1973.
17. T. Lindeberg, *Scale-Space Theory in Computer Vision*. The Kluwer International Series in Engineering and Computer Science, Kluwer Academic Publishers: Dordrecht, The Netherlands, 1994.
18. D.C. Marr and E.C. Hildreth, "Theory of edge detection," in *Proceedings of the Royal Society of London, B*, Vol. 207, pp. 187–217, 1980.
19. C.W. Misner, K.S. Thorne, and J.A. Wheeler, *Gravitation*, Freeman: San Francisco, 1973.
20. M. Nielsen, L.M.J. Florack, and R. Deriche, "Regularization, scale-space and edge detection filters" *Journal of Mathematical Imaging and Vision*, Vol. 7, No. 4, pp. 291–307, 1997.
21. P.J. Olver, *Applications of Lie Groups to Differential Equations*, Springer-Verlag, 1986. Vol. 107 of *Graduate Texts in Mathematics*.
22. N. Otsu, "*Mathematical Studies on Feature Extraction in Pattern Recognition*," Ph.D. thesis, Electrotechnical Laboratory, Ibaraki, Japan, 1981. (in Japanese).
23. J. Smoller, "Shock Waves and Reaction-Diffusion Equations," Grundlehren der mathematischen Wissenschaften. Springer-Verlag: New York, 1994.
24. J. Sporring, M. Nielsen, L.M.J. Florack, and P. Johansen (Eds.), *Gaussian Scale-Space Theory*, Vol. 8 of *Computational Imaging and Vision Series*. Kluwer Academic Publishers: Dordrecht, The Netherlands, 1997.
25. A.P. Witkin, "Scale-space filtering," in *Proceedings of the International Joint Conference on Artificial Intelligence*, Karlsruhe, Germany, 1983, pp. 1019–1022.

Luc Florack received his M.Sc. degree in theoretical physics in 1989, and his Ph.D. degree in 1993 with a thesis on image structure, both from Utrecht University, The Netherlands. During the period 1994–1995 he was an ERCIM/HCM research fellow at INRIA Sophia-Antipolis, France, and INESC Aveiro, Portugal. In 1996 he was an assistant research professor at DIKU, Copenhagen, Denmark, on a grant from the Danish Research Council. Since 1997 he has been a researcher at Utrecht University, first at the Department of Computer Science, and subsequently at the Department of Mathematics. His interest subtends all structural aspects of signals, images and movies, notably multiscale representations, and their applications to imaging and vision.